Dynamical activities of primary somatosensory cortices studied by magnetoencephalography

Kuniharu Kishida*
Department of Information Science, Faculty of Engineering, Gifu University, 1-1 Yanagido Gifu, 501-1193, Japan
(Received 23 February 2009; revised manuscript received 3 October 2009; published 6 November 2009)

A blind identification method of transfer functions in feedback systems is introduced for examination of dynamical activities of cortices by magnetoencephalography study. Somatosensory activities are examined in 5 Hz periodical median nerve stimulus. In the present paper, we will try two careful preprocessing procedures for the identification method to obtain impulse responses between primary somatosensory cortices. Time series data of the somatosensory evoked field are obtained by using a blind source separation of the T/k type (fractional) decorrelation method. Time series data of current dipoles of primary somatosensory cortices are transformed from the time series data of the somatosensory evoked field by the inverse problem. Fluctuations of current dipoles of them are obtained after elimination of deterministic periodical evoked waveforms. An identification method based on feedback system theory is used for estimation of transfer functions in a feedback model from obtained fluctuations of currents dipoles of primary somatosensory cortices. Dynamical activities between them are presented by Bode diagrams of transfer functions and their impulse responses: the time delay of about 30 ms via corpus callosum is found in the impulse response of identified transfer function.

DOI: 10.1103/PhysRevE.80.051906 PACS number(s): 87.19.−j, 02.50.−r, 05.40.−a, 87.50.−a

I. INTRODUCTION

Evoked magnetic fields are often used to examine brain activities [1] although amplitudes of evoked magnetic fields are smaller than those of spontaneous magnetic fields. Averaged waveforms of magnetoencephalography (MEG) are used usually to examine the evoked magnetic fields. Though we can obtain dynamical information from averaged waveforms, we may find a possibility to obtain dynamical information from fluctuations about the averaged waveforms. Hence, there remains a methodology to obtain dynamical information of brain activities in MEG analysis. In a previous paper [2], periodical responses of evoked magnetic fields were studied for 5 Hz periodical median nerve stimuli. As statistical properties of the somatosensory evoked field (SEF) were reported in [2], SEF has the deterministic part of periodical averaged waveforms and the random part of fluctuations around them. The aim of present paper is to obtain dynamical information from SEF fluctuations.

There are two state-of-the-art approaches for understanding connections among brain regions. One approach tries to model how activity in one brain area is affected by that in another. The other approach looks for correlations in activities of two or more regions. In the present paper we use the latter approach. To obtain dynamical information of MEG and/or electroencephalography data multivariate autoregressive models have been used mainly for identification of networks or connections between cortices as in [3,4] and references cited therein. However, they are all-pole type of models and have no zeros. Since autoregressive models are a kind of truncated power series as in [5], they are not suitable to evaluate exactly transfer functions between cortices. To avoid this difficulty we will use a blind identification by an innovation model with minimum phase properties. An identification method based on feedback system theory [6,7] will be used for determination of impulse responses between cortices.

With 5 Hz periodic median nerve stimulus, somatosensory activity is mainly observed [8] at the primary somatosensory cortex in the contralateral hemisphere (cSI), although for random stimuli with interstimulus intervals of more than 1 s, somatosensory activities are known [9] as cSI, bilateral secondary somatosensory cortices, and posterior parietal cortices. Not only contralateral but also ipsilateral responses in primary somatosensory cortex following 5 Hz electrical median nerve stimulation were reported [10,11] in functional magnetic resonance imaging. However, ipsilateral primary somatosensory (iSI) responses to median nerve stimulation are rare in MEG investigation as reported by Kanno *et al.* [12]: 18 hemispheres of 14 among 482 subjects. Furthermore, the pathway of the ipsilateral response is unclear. There are three possibilities: (1) transcallosal type from cSI cortex; (2) direct afferent projection type from thalamus; and (3) top-down type from higher-level processing areas. This is still remaining an open problem. In [13] averaged waveforms of current dipoles of primary somatosensory cortexes were studied from electroencephalography via the decorrelation method of the blind source separation (BSS) method. The usage of the decorrelation method can make an improvement on the signal-to-noise (S/N) ratio of components of interest. In the present paper SEF fluctuations of the somatosensory evoked field will be separated from MEG data by using the T/k type decorrelation method of BSS after elimination of deterministic periodical evoked waveforms. A pathway of transcallosal type of (1) will be reported by application of an identification method based on feedback system theory [6,7] to SEF fluctuations.

Separation of somatosensory evoked field will be mentioned in Sec. II. Lead field, BSS, and estimation of current dipoles of cSI and iSI will be discussed for inverse transformation of time series data from superconducting quantum interference devices (SQUIDs) to current dipoles of somatosensory cortices. Identification of dynamical activities be-

*kishida@gifu-u.ac.jp

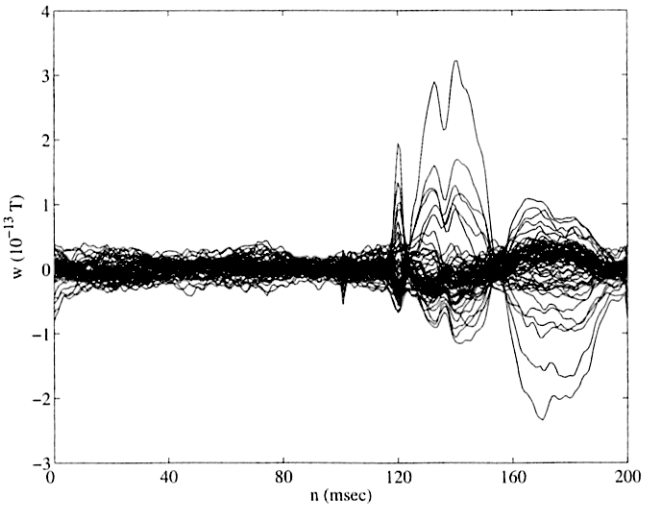

FIG. 1. Averaged waveforms $w(n)$ of MEG.

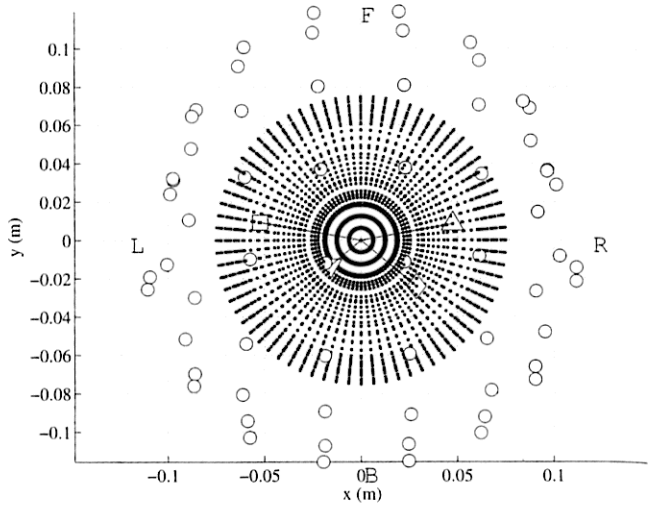

FIG. 2. Location of SQUIDs and current dipoles in the MEG head coordinates. Letters of F, B, L, and R in the figure mean front, back, left, and right, respectively.

tween primary somatosensory cortices will be discussed in Sec. III.

II. SEPARATION OF SOMATOSENSORY EVOKED FIELD IN MAGNETOENCEPHALOGRAPHY

Seven healthy subjects participated in this paper. After explaining the nature of the study, informed consent has been obtained. The experimental procedures were in accordance with the declaration of Helsinki. For them the median nerve was stimulated electrically with a constant voltage, square-wave pulse of 0.2 ms duration delivered at the right wrist. Stimulus frequency was periodical 5 Hz or the interstimulus interval was 200 ms. MEG data were recorded with a 64-channel whole-head MEG system (NeuroSQUID Model 100; CTF Systems Inc.). SQUID was the axial gradiometer type. MEG signals were digitized at 1250 Hz and filtered with a 300 Hz on-line low-pass filter. MEG data during 100 s were recorded as a single sweep. The number of median nerve stimuli was 500. Details were reported in [2].

After zero preset signal processing mentioned in [2] the average of 500 responses of MEG was used. The averaged waveforms $w(n)$ are obtained from SQUID time series data and shown in Fig. 1 for one subject, where $w(n)$ were defined by Eq. (1) of [2]. The electric stimulus time is at time 100.8 ms in Fig. 1. The first peak of waveform at time 120 ms is known as N20 with latency 19.2 ms [1,8,9].

A. Lead field

The magnetic field can be calculated from Maxwell equations. Especially, the forward problem from a current in a head to a SQUID channel is evaluated by the Biot-Savart law or Ampere-Laplace law. If the head can be well approximated by a spherically symmetric model and if the primary currents generated in the brain can be described by an equivalent current dipole, a lead field from a current dipole in the brain to SQUID channels was given by Sarvas formula [14].

Current dipoles in a brain were uniformly distributed in the sphere with a radius 0.075 m at a center (0, 0, 0.05) (meter) in the MEG head coordinates. They are expressed by tiny symbol of square in Figs. 2 and 3. The number of them was 9514. Large circles in Figs. 2 and 3 are 64 SQUIDs.

Let a current dipole at a position $r \in N(1 \leq r \leq 9514)$ in the brain be denoted by $\boldsymbol{Q}_r(n)$ at discrete time n. In the tangential plane at the position r a current dipole with angle θ is denoted by $\boldsymbol{Q}_r(n) := Q_r(n)(\cos\theta \boldsymbol{i} + \sin\theta \boldsymbol{j}) = Q_r(n,x)\boldsymbol{i} + Q_r(n,y)\boldsymbol{j}$, where $\boldsymbol{i}$ and $\boldsymbol{j}$ are unit vectors in the tangential plane.

From the Sarvas formula the magnetic field from a unit dipole of x direction at r to the mth channel of SQUID can be given by $l_m(r,x)$. The magnetic field at SQUIDs are determined by

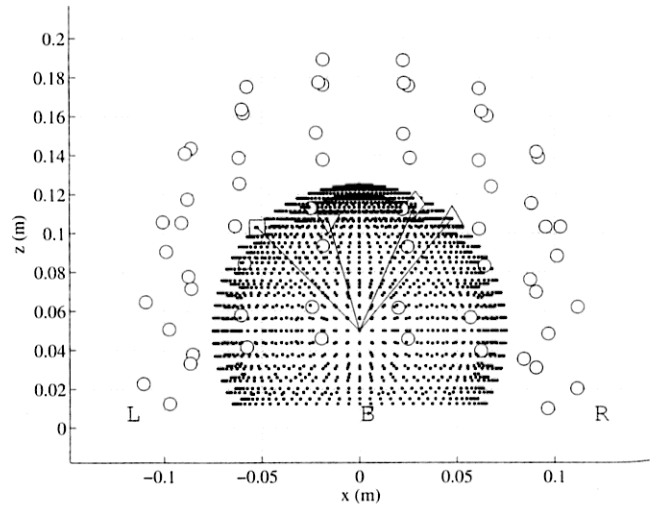

FIG. 3. Location of 64 SQUIDs and current dipoles in the MEG head coordinates.

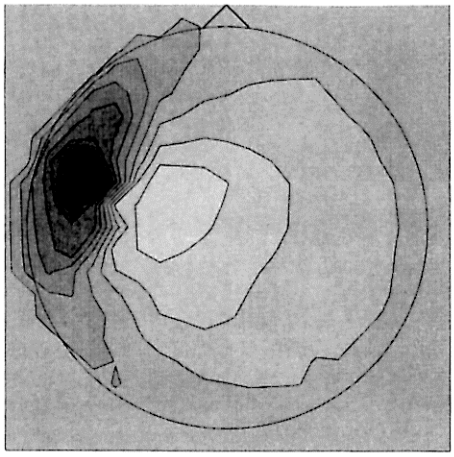

FIG. 4. (Color online) Dipole pattern generated by a current dipole at position 8618 (cSI).

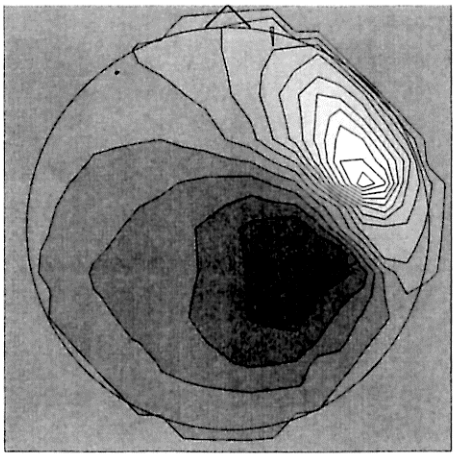

FIG. 5. (Color online) Dipole pattern generated by a current dipole at position 7851 (iSI).

$$\boldsymbol{b}(n) = \sum_{r=1}^{9514} \boldsymbol{l}_r \boldsymbol{Q}_r(n), \tag{1}$$

where $\boldsymbol{b}(n)$ are time series data of magnetic field at positions of SQUID:

$$\boldsymbol{b}(n) := \begin{pmatrix} b_1(n) \\ b_2(n) \\ \vdots \\ b_{64}(n) \end{pmatrix}, \quad \boldsymbol{Q}_r(n) := \begin{pmatrix} Q_r(n,x) \\ Q_r(n,y) \end{pmatrix}$$

and

$$\boldsymbol{l}_r := \begin{pmatrix} l_1(r,x) & l_1(r,y) \\ l_2(r,x) & l_2(r,y) \\ \vdots & \vdots \\ l_{64}(r,x) & l_{64}(r,y) \end{pmatrix},$$

or we have

$$\boldsymbol{b}(n) = \boldsymbol{L}\boldsymbol{Q}(n), \tag{2}$$

where

$$\boldsymbol{L} := (\boldsymbol{l}_1, \boldsymbol{l}_2, \ldots, \boldsymbol{l}_{9514}), \boldsymbol{Q}(n) := \begin{pmatrix} \boldsymbol{Q}_1(n) \\ \boldsymbol{Q}_2(n) \\ \vdots \\ \boldsymbol{Q}_{9514}(n) \end{pmatrix}.$$

For example, a current dipole with angle 175.14° at position 8618 in the brain generates a dipole pattern at SQUID positions. The location of the current dipole is given by the symbol of □ in Figs. 2 and 3 and its dipole pattern of $\boldsymbol{b}_{8618} = \boldsymbol{l}_{8618}\boldsymbol{Q}_{8618}$ is shown in Fig. 4. Amplitudes of outgoing or incoming magnetic fields are given by contours from black to white color scale in the figure. Details of isofield map of dipole patterns have been reported in [15]. A current dipole with angle 40.93° at position 7851 (the symbol of △ in Figs. 2 and 3) also generates a dipole pattern of $\boldsymbol{b}_{7851} = \boldsymbol{l}_{7851}\boldsymbol{Q}_{7851}$ shown in Fig. 5.

B. Blind source separation

To retrieve MEG of SEF, we have used the second-order correlation functions for periodical types of blind source separation, i.e., the decorrelation method of BSS. The decorrelation method was developed by Molgedey and Schuster [16], Ziehe *et al.* [17], and Murata *et al.* [18] and briefly summarized in [19]. However, BSS performance is strongly dependent on the choice of time delayed parameters. The temporal decorrelation method of BSS has an open problem in choice of the time delayed parameters [17,20,21].

Since PSD of MEG has a line spectrum of 5 Hz and its repeated higher harmonic modes in 5 Hz periodical median nerve stimuli, improvements with fractional-type time-delayed parameters τ_m defined by

$$\text{T/k type: } \tau_m = \left(\frac{1250}{5}\right)/m = \frac{250}{m}, \quad m = 1,2,\ldots,k. \tag{3}$$

could be made on the BSS as mentioned in [2,22]. Hence, we can determine a matrix $A_{(k)}$ by the blind source separation with T/k-type (fractional) time delays:

$$\boldsymbol{x}(n) = A_{(k)}\boldsymbol{s}^{(k)}(n), \tag{4}$$

where $\boldsymbol{x}(n)$ is measured SQUID data of magnetic field with artifact noises of blinks, power electrical noise and so forth at 64 SQUID channels, $\boldsymbol{s}^{(k)}(n)$ is a vector of normalized components of BSS. In the decorrelation method, the absolute sum of off-diagonal elements of normalized correlation matrices are minimized at times corresponding to 5 Hz and its higher harmonic frequencies.

To extract 5 Hz periodical components of BSS we have used the T/k type of BSS with $k=7$:

$$\boldsymbol{x}(n) = A_{(7)}\boldsymbol{s}^{(7)}(n).$$

For $k=8$ we also have

$$\boldsymbol{x}(n) = A_{(8)}\boldsymbol{s}^{(8)}(n).$$

From the above two relations we can determine a distribution matrix $T := A_{(8)}^{-1}A_{(7)}$ from $\boldsymbol{s}^{(7)}(n)$ to $\boldsymbol{s}^{(8)}(n)$. The jth column of T shows a distribution of the jth component of $\boldsymbol{s}^{(7)}(n)$, $s_j^{(7)}(n)$,

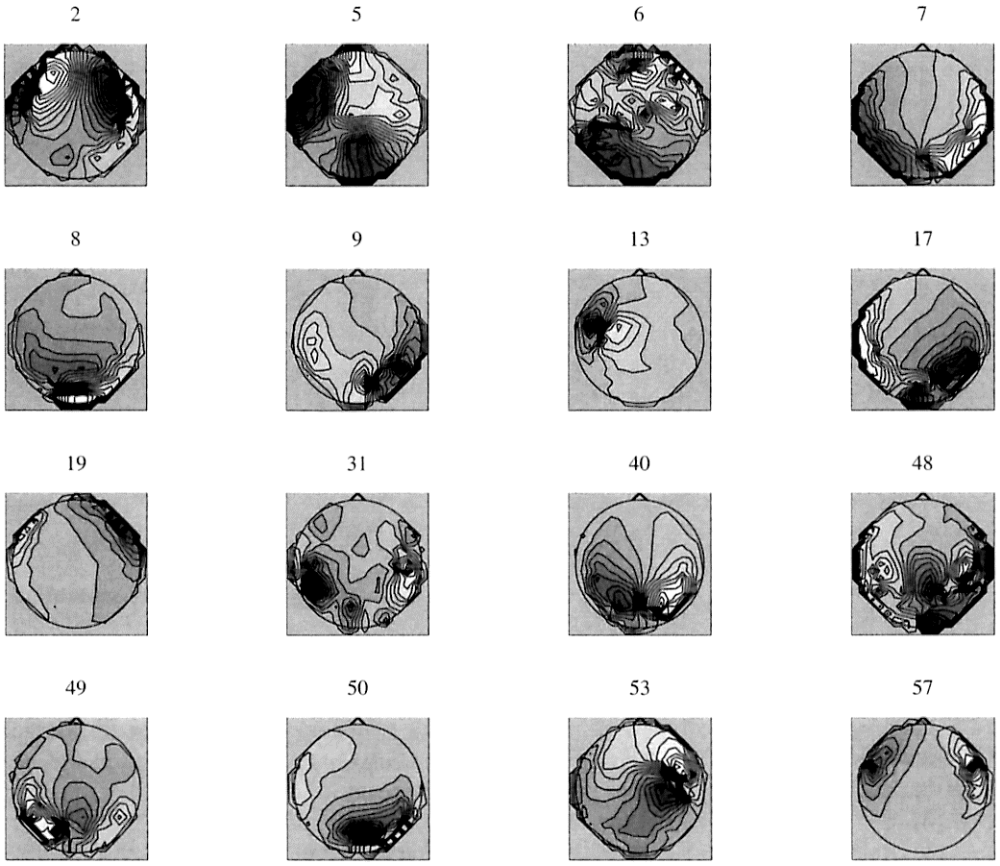

FIG. 6. (Color online) Dominant dipole patterns of BSS.

in $s^{(8)}(n)$ and is denoted by $T_{*,j}$. When components of BSS satisfy the condition that absolute value of $T_{*,j}$ is close to one, the BSS components are robust for decomposition by BSS. That is, if the decompositions for $k=7$ and $k=8$ were consistent then T would be approximately a permutation matrix so that in each column of T there should be a dominant element with absolute value close to 1. A component is considered robust if the corresponding column vector of T resembles a column of a permutation matrix without regard to the other columns.

We found two subjects with robust BSS components corresponding to activities near iSI from seven subjects. In one of two subjects, however, the pattern of obtained iSI dipole was rotated by about 90° in comparison with that of anatomical iSI dipole. Hereafter we will examine the other subject with the averaged waveforms of Fig. 1 in the remaining part of the present paper. If the components of BSS satisfy the condition $|T_{*,j}|>0.98$, the components are robust for BSS. Sixteen components of BSS were robust, and their dipole patterns are shown in Fig. 6. Here, a dipole pattern of the jth component of BSS is given from the jth column vector of $A_{(7)}$ as mentioned in [15]. The robust components of BSS were classified into four groups by examination of their power spectral densities: (i) electric power noises; the fifth and sixth components of BSS, (ii) eye movement or blinks; the second, 19th, and 57th components of BSS, (iii) α wave; the seventh, eighth, ninth, 17th, 31st, 40th, 48th, 49th, and 50th components of BSS, (iv) SEF; the 13th and 53rd components of BSS. These results of SEF are consistent to those of [8], in which second somatosensory cortices and posterior parietal cortices were not observed as active portions of SEF in 5 Hz periodical median nerve stimulus.

Since a dipole pattern at time 172 ms of the waveforms in Fig. 1 is shown in Fig. 7, the similarity between the dipole pattern and that of the 13th component of BSS means that the 13th component of BSS relates to the current dipole of the contralateral primary somatosensory cortex. Here, cSI in time 172 ms of latency 71.2 ms are considered to be active. The 53rd component of BSS will be examined in discussion

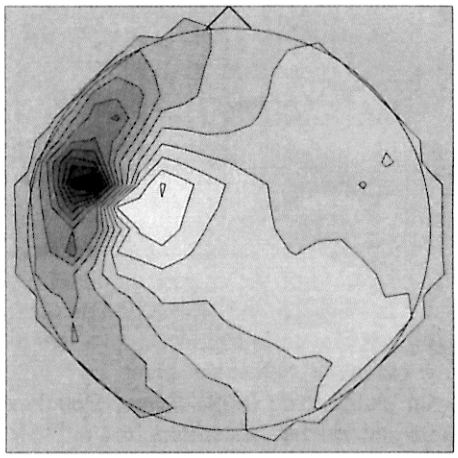

FIG. 7. (Color online) Dipole pattern of $\boldsymbol{w}(n)$ at time 172 ms of Fig. 1.

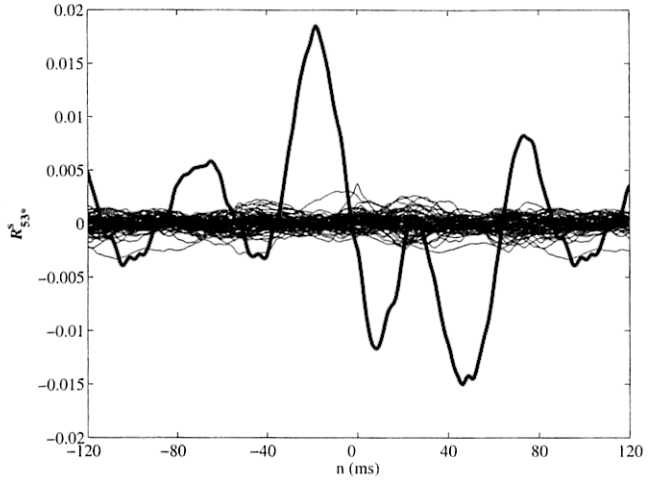

FIG. 8. Pseudocorrelation functions $R^s_{53*}(n)$ of repeated waveforms between the 53rd and the other components of BSS.

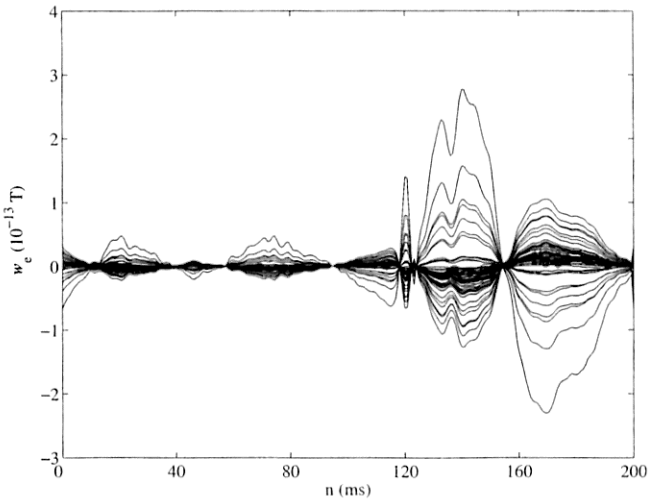

FIG. 9. SEF waveforms, $\boldsymbol{w}_e(n)$.

(2), and it relates to the current dipole of the ipsilateral primary somatosensory cortex.

Let averaged waveforms of BSS components be $\boldsymbol{w}^s(n)$. Let us examine pseudocorrelation functions of repeated waveforms between the 53rd BSS component and the other BSS component defined as in Eq. (7) of [2] by

$$R^s_{53*}(n) := pC\{r_M \boldsymbol{w}^s_{53}(0), r_M \boldsymbol{w}^s_*(n)\}, \tag{5}$$

where $r_M \boldsymbol{w}^s$ are defined by concatenating 500 copies of the averaged waveforms $\boldsymbol{w}^s$. Pseudo-correlation functions of repeated waveforms between the 53rd BSS component and the other BSS components, $R^s_{53*}(n)$, are shown in Fig. 8.

The bold line in Fig. 8 is a dominant pseudocorrelation between the 13th and the 53rd components of BSS. Therefore SEF can be rebuilt from the 13th and 53rd components of BSS for brain activities of cSI and iSI as mentioned in [2].

By selecting two BSSs in the subject SQUID time series data of somatosensory evoked magnetic field, $\boldsymbol{b}_e(n)$, generated from somatosensory cortexes can be separated from background brain noise of MEG data since SEF are generated from currents of cortices related to somatosensory activities:

$$\boldsymbol{b}_e(n) = A_{(7)} \boldsymbol{s}^{(7)}_e(n). \tag{6}$$

Here $\boldsymbol{s}^{(7)}_e$ indicates that the 13th and 53rd components of BSS with $k=7$ leave the original ones and the other 62 components of BSS are set as zero vectors.

Averaged waveforms $\boldsymbol{w}_e(n)$ of SEF on SQUIDs can be obtained from $\boldsymbol{b}_e(n)$ and shown in Fig. 9. The similarity between Figs. 1 and 9 teaches us that it is successful to extract $\boldsymbol{b}_e(n)$ from $\boldsymbol{x}(n)$.

C. Estimation of current dipoles of cSI and iSI

The number of SQUIDs was 64, and let the number of active portions in a brain be r. When we want to examine brain activities, we must solve the inverse problem of r from 64. Since there are a lot of background activities in the brain, usually $64 \ll r$, that is, we must solve the underdetermined problem to examine brain activities. In general it is difficult to examine brain activities from SQUID time series data inversely. Let the number of active portions in a brain be p in the case of evoked magnetic field. Instead of SQUID time series data, $\boldsymbol{x}(n)$, we can analyze SEF time series data, $\boldsymbol{b}_e(n)$, generated by a few active portions in the brain, usually $p < 64$. That is, to examine brain activities of cortices evoked by stimuli is a kind of the overdetermined problem.

The multidipole estimation is carried out by the least-squares method [1]. Though it is hard to seek the minimum in the conventional least-squares method of multidipole, the problem can be solved by the conventional least-squares method with the combinatory optimization problem for location of current dipoles. Estimated current dipoles were equivalently evaluated by the least-squares method with a cost function of distance between signal spaces [23]. That is, the covariance matrix, $\boldsymbol{D} = E\{\boldsymbol{b}_e(n)\boldsymbol{b}_e(n)^T\}$, can be decomposed into eigenvectors:

$$\boldsymbol{D} = \sum_{k=1}^{64} \lambda_k \phi_k \phi_k^T, \tag{7}$$

where the superscript T denotes the transposition of matrix, λ_k is an eigenvalue, and ϕ_k is its eigenvector. Let us divide two subspaces; one is the signal subspace $\boldsymbol{V}_s$ and the other subspace is noise subspace $\boldsymbol{V}_n$:

$$\boldsymbol{V}_s = (\phi_1, \phi_2, \ldots, \phi_q), \quad \boldsymbol{V}_n = (\phi_{q+1}, \phi_{q+2}, \ldots, \phi_{64}),$$

where $p \le q$. For q current dipole estimation the cost function of combined subspaces $(\boldsymbol{V}_s, \boldsymbol{L}_{\hat{\boldsymbol{r}}})$ is defined [23] by

$$J(\hat{\boldsymbol{r}}_1, \ldots, \hat{\boldsymbol{r}}_{\hat{q}}) = \det[(\boldsymbol{V}_s, \boldsymbol{L}_{\hat{\boldsymbol{r}}})^T (\boldsymbol{V}_s, \boldsymbol{L}_{\hat{\boldsymbol{r}}})], \tag{8}$$

where

$$\boldsymbol{L}_{\hat{\boldsymbol{r}}} := (\boldsymbol{l}_{\hat{r}_1}, \boldsymbol{l}_{\hat{r}_2}, \ldots, \boldsymbol{l}_{\hat{r}_q}).$$

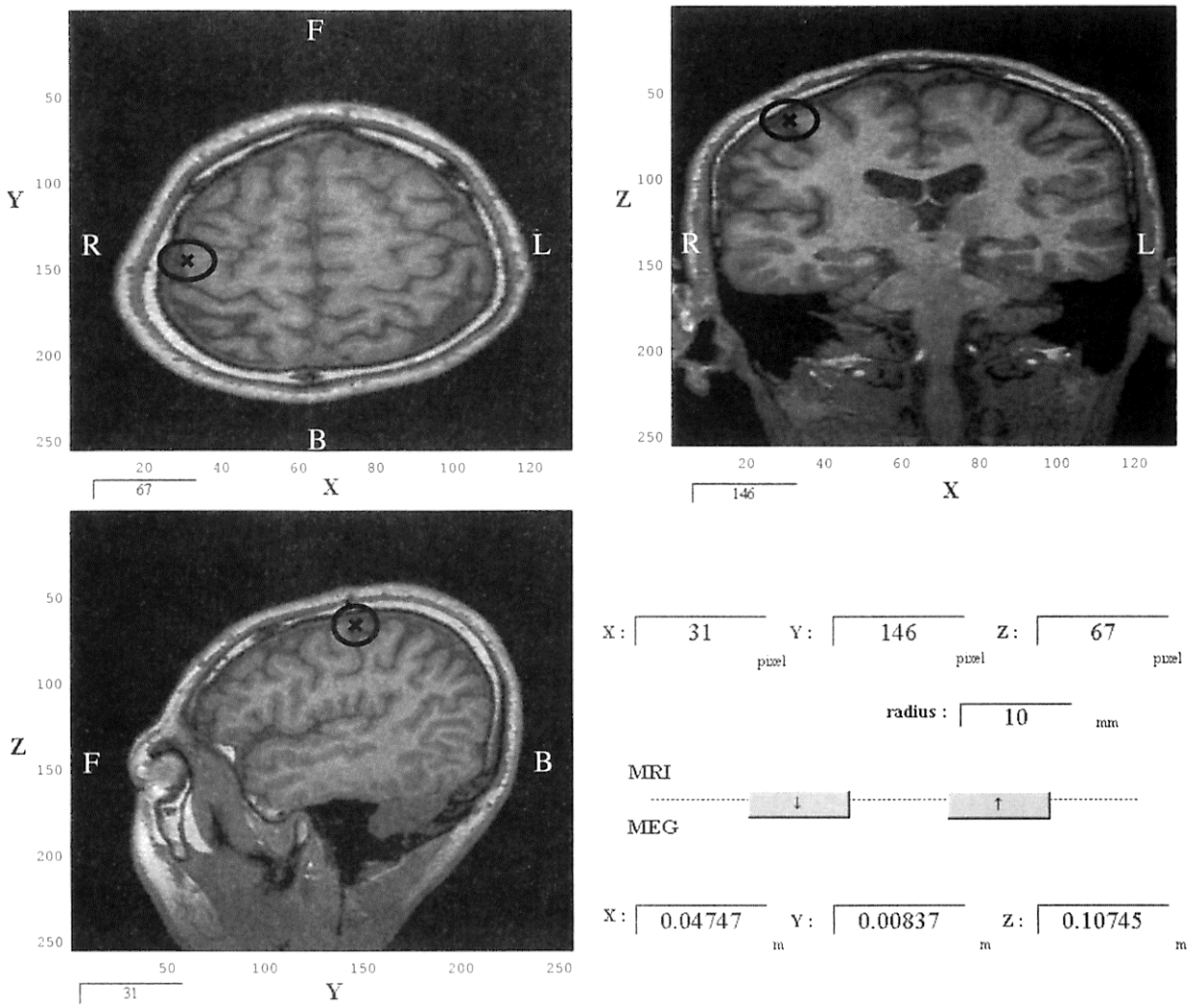

FIG. 10. Location of position 7851 (iSI) in MRI presentation. Letters of F, B, L, and R in the figure mean front, back, left, and right, respectively.

The effective reason of cost function is that the rank of $[(\boldsymbol{V}_s,\boldsymbol{L}_{\hat{r}})^T(\boldsymbol{V}_s,\boldsymbol{L}_{\hat{r}})]$ becomes lower when estimation of current dipole is true. Hence, we could solved the problem of multidipole estimation by the conventional least-squares method with the combinatory optimization problem for location of current dipoles. Furthermore, our least-squares method works even in the case of correlated dipoles [23] although the assumption of independent dipoles is needed in the multiple signal classification (MUSIC) method [24].

A source space defined by a set of possible dipoles located on 9514 points was used for the four current dipole estimation (q=4). In the four current dipole estimation SEF signals, $\boldsymbol{b}_e(n)$, are assumed to be generated by four SEF portions in the brain.

Four current dipoles were estimated from the abovementioned method. The 77.8 percentage of covariance matrix of D could be expressed by four current dipoles. Four current dipoles at position 3676 with angle 85.47°, position 7851 with angle 40.93°, position 8618 with angle 175.14 degrees and position 9341 with 126.24° are shown by symbols ▽, △, □, and ◇, respectively, in Figs. 2 and 3. Especially, two current dipoles at positions 7851 and 8618 had larger amplitudes than the other current dipoles. The location of positions 7851 and 8618 are superimposed on MRI slices in Figs. 10 and 11. Here MRI of the subject had 130 slices with 256×256 pixels. The position 7851 of symbol △ in Figs. 2 and 3 is (0.047 47, 0.008 37, 0.107 45) (meter) in the MEG head coordinates, and (31, 146, 67) (pixel) in the MRI coordinates. The position is denoted by symbol × surrounded by a black circle in Fig. 10. The position of 7851 in MRI is the iSI. The position 8618 of symbol □ at (−0.052 23, 0.009 209, 0.103 033) (meter) corresponds to that of (102, 141, 64) [pixel] in Fig. 11. The position of 8618 in MRI is the cSI.

From the SEF signals of Eq. (6) we can obtain scalar time series data of four current dipoles by using lead fields of them:

$$Q_e(n) = \boldsymbol{L}_e^{\dagger}\boldsymbol{b}_e(n), \tag{9}$$

where the symbol † means the Moore-Penrose type of generalized inverse matrix,

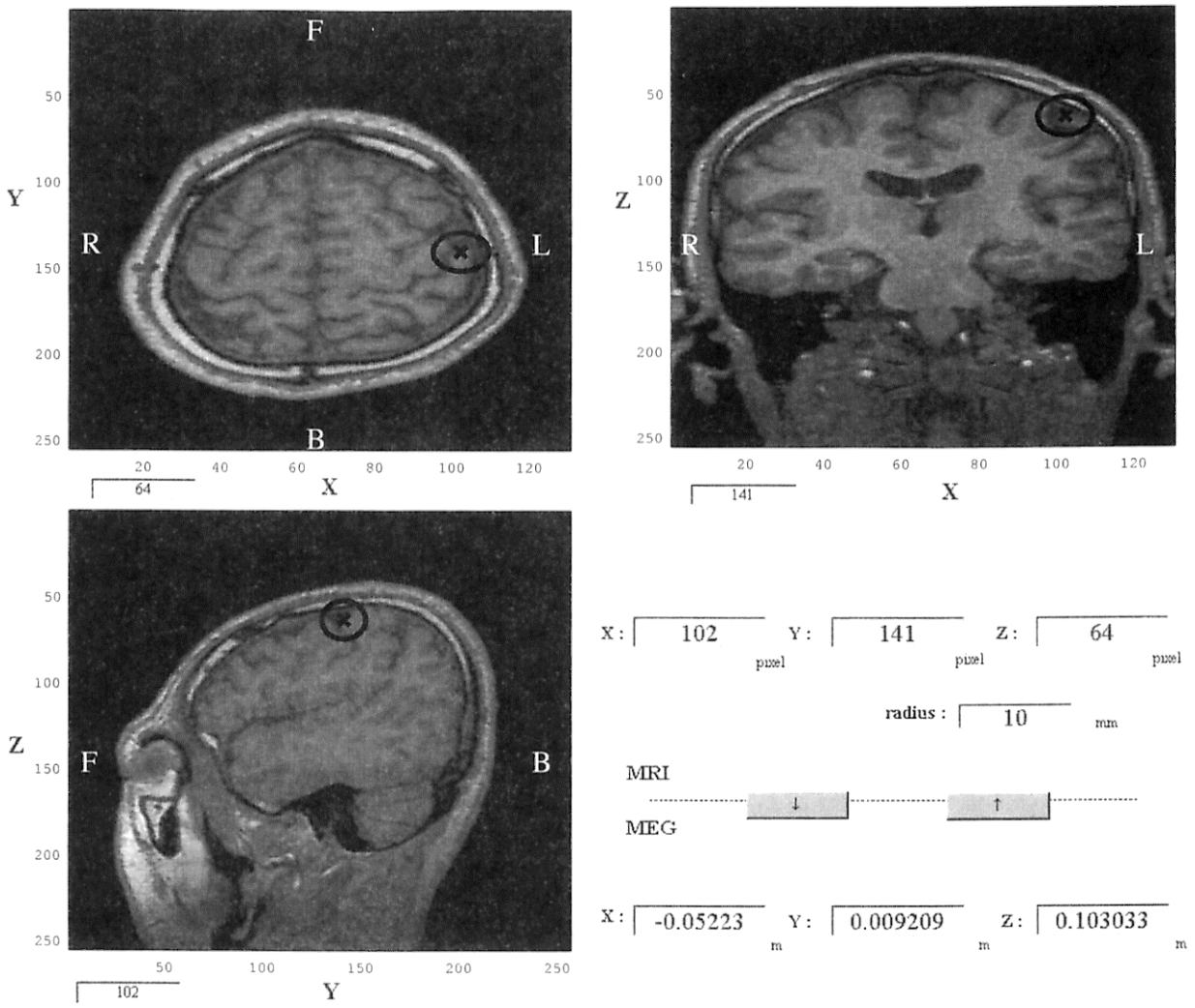

FIG. 11. Location of position 8618 (cSI) in MRI presentation. Letters of F, B, L, and R in the figure mean front, back, left, and right, respectively.

$$Q_e(n) := \begin{pmatrix} Q_{3676}(n) \\ Q_{7851}(n) \\ Q_{8618}(n) \\ Q_{9341}(n) \end{pmatrix}, \quad \boldsymbol{L}_e = (\underline{l}_{3676}, \underline{l}_{7851}, \underline{l}_{8618}, \underline{l}_{9341}),$$

with

$$\underline{l}_* := \begin{pmatrix} l_1(*,x)\cos\theta_* + l_1(*,y)\sin\theta_* \\ l_2(*,x)\cos\theta_* + l_2(*,y)\sin\theta_* \\ \vdots \\ l_{64}(*,x)\cos\theta_* + l_{64}(*,y)\sin\theta_* \end{pmatrix},$$

Finally averaged waveforms of cSI and iSI can be obtained from current dipoles of $[Q_{7851}(n)Q_{8618}(n)]^T$ and shown in Fig. 12. Here amplitudes of cSI and iSI in Fig. 12 are not exact in the four current dipole estimation since we have used the pseudoinverse matrix in Eq. (9). Waveform of cSI is expressed by a solid line and that of iSI is a broken line in Fig. 12.

III. IDENTIFICATION OF DYNAMICAL ACTIVITIES BETWEEN PRIMARY SOMATOSENSORY CORTICES IN SEF

Let $\boldsymbol{w}_e^Q$ be averaged waveforms of Q_{7851} and Q_{8618}. When $r_{500}\boldsymbol{w}_e^Q$ is defined by concatenating 500 copies of the averaged waveforms $\boldsymbol{w}_e^Q$, we have SEF fluctuations of $y_1(n)$ for iSI and $y_2(n)$ for cSI;

$$\boldsymbol{y}(n) = [y_1(n)y_2(n)]^T := [Q_{7851}(n)Q_{8618}(n)]^T - r_{500}\boldsymbol{w}_e^Q. \tag{10}$$

Hence we can obtain dynamical information from stationary time series data $\boldsymbol{y}(n)$ by using an identification method of feedback system theory [6,7].

From evaluated SEF fluctuations of Eq. (10) let us identify dynamics of iSI and cSI activities with a feedback model defined by

$$y_1(n) = F_{12}(z^{-1})y_2(n) + F_1(z^{-1})f_1(n),$$

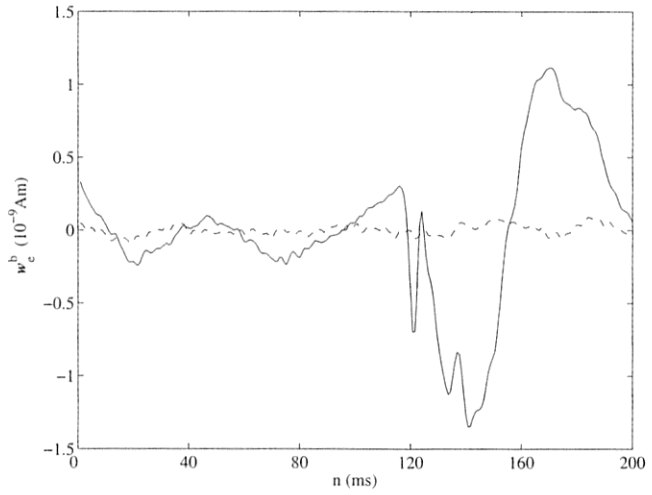

FIG. 12. Averaged waveforms of cSI (solid line) and iSI (broken line).

$$y_2(n) = F_{21}(z^{-1})y_1(n) + F_2(z^{-1})f_2(n), \tag{11}$$

where z^{-1} is the time shift operator: $z^{-1}\boldsymbol{y}(n)=\boldsymbol{y}(n-1)$, $f_1(n)$ and $f_2(n)$ are Gaussian white random current dipoles in right (ipsilateral) and left (contralateral) thalami, $F_{12}(z^{-1})$ is a transfer function between cortices from cSI to iSI via the corpus callosum, and $F_{21}(z^{-1})$ is a reverse transfer function from iSI to cSI. $F_1(z^{-1})$ is a transfer function from right thalamus to iSI and $F_2(z^{-1})$ is that from left thalamus to cSI.

As will be mentioned in Eq. (A3) we can identify an innovation model of minimum phase from time series data of SEF fluctuations $\boldsymbol{y}(n)$;

$$\boldsymbol{x}(n|n) = A_H\boldsymbol{x}(n-1|n-1) + B\gamma(n).$$

$$\boldsymbol{y}(n) = C\boldsymbol{x}(n|n). \tag{12}$$

From Eq. (12) we have a closed loop transfer function matrix,

$$G(z^{-1}) = C(I - A_H z^{-1})^{-1}B. \tag{13}$$

Here the number of singular values of Hankel matrix in step 3 of Appendix A was 22 in determination of the data-oriented innovation model.

As will be mentioned in Eq. (B3) transfer functions between iSI and cSI are determined from Eq. (13) as

$$\hat{F}_{12}(z^{-1}) = G_{12}(z^{-1})G_{22}(z^{-1})^{-1},$$

$$\hat{F}_{21}(z^{-1}) = G_{21}(z^{-1})G_{11}(z^{-1})^{-1}, \tag{14}$$

where

$$G(z^{-1}) =: \begin{pmatrix} G_{11}(z^{-1}) & G_{12}(z^{-1}) \\ G_{21}(z^{-1}) & G_{22}(z^{-1}) \end{pmatrix}. \tag{15}$$

The bode diagrams of $\hat{F}_{12}(z^{-1})$, $\hat{F}_{21}(z^{-1})$ and their impulse responses are shown in Figs. 13 and 14. The upper and middle figure is the magnitude and the phase of Bode diagram of each transfer function, and the lower figure is the impulse response.

A model reduction algorithm is needed in evaluation of transfer functions numerically [25] since there occurs a cancellation in poles and zeros of identified transfer functions.

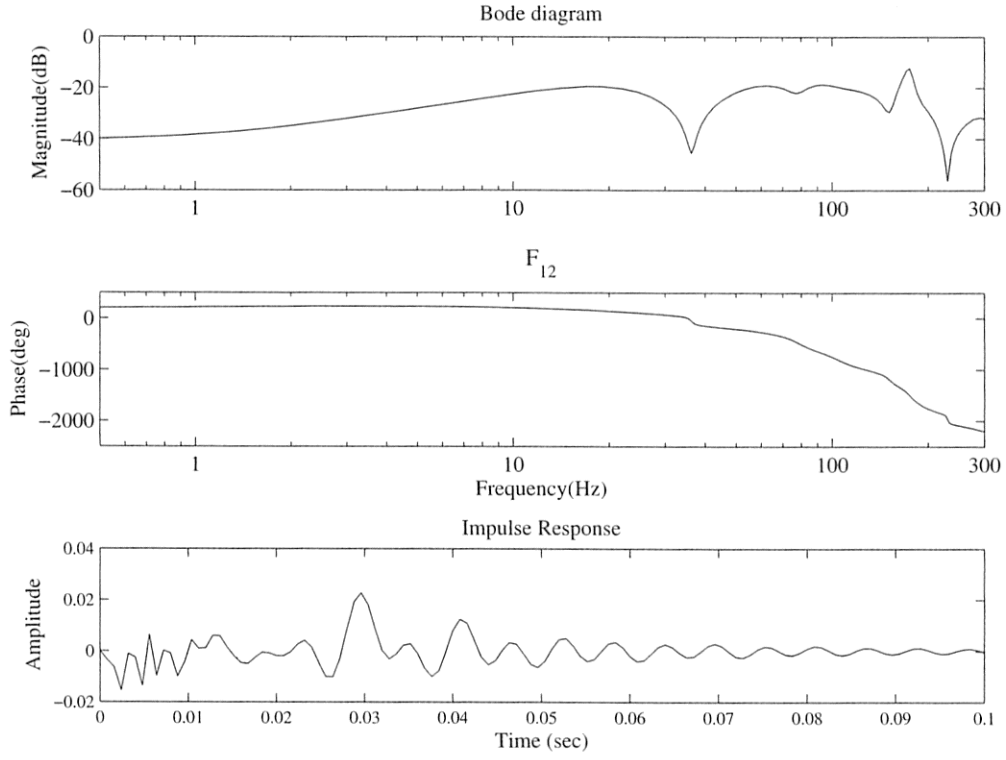

FIG. 13. Bode diagram of $\hat{F}_{12}$ from cSI to iSI and its impulse response.

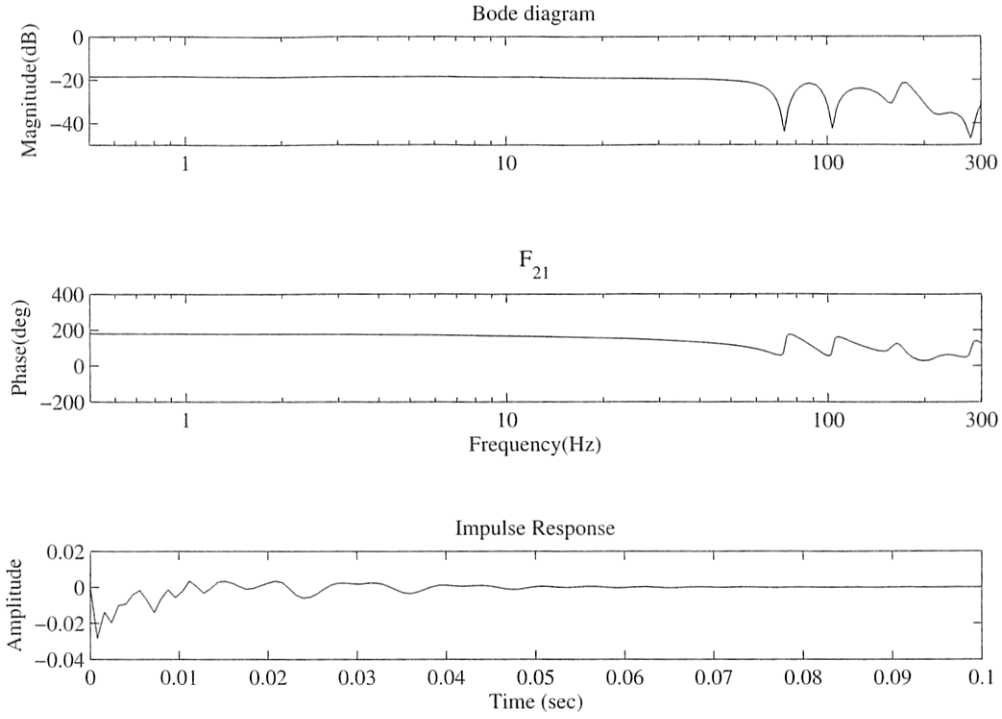

FIG. 14. Bode diagram of $\hat{F}_{21}$ from iSI to cSI and its impulse response.

In the impulse response of Fig. 13 we can find the time delay via the corpus callosum. The time delay is expressed approximately by the rational function of z^{-1}, $F_{12}(z^{-1})$. We have detected find the time delay from cSI to iSI in the fluctuation analysis of MEG. As mentioned in [26] this time delay of about 30 ms may be expressed as follows: after activation of the contralateral area 3b, areas 1 and 2 on the same side are activated via anteroposterior corticocortical projections. The ipsilateral SI area can obtain signal through transcallosal connections (its transit time ~20 ms), most likely via area 2, which has the denest transcallosal connections among all SI areas.

We can see the similar order of time delay in the waveform level of Fig. 12, although the first peak of N20 of cSI is time 120 ms and that of iSI is 138.4 ms.

IV. DISCUSSION

(1) For another data measured from the same subject we checked the reproducibility of $F_{12}(z^{-1})$ from cSI to iSI in the right median nerve stimulus. Here, the additional data were obtained on a different occasion, and not in the same recording session. The number of median nerve stimuli was 100 in the time series data. The other experimental conditions were the same as those in Sec. II. Via two procedures of BSS and inverse problem from SQUID to current dipoles we could obtain the additional SEF fluctuations after elimination of periodical evoked waveforms. To evaluate transfer functions the number of singular values of Hankel matrix was 25 in determination of the data-oriented innovation model of the addition case. We obtained the bode diagrams of $\hat{F}_{12}(z^{-1})$ and their impulse responses in Fig. 15. The time delay of about 30 ms could be detected in Fig. 15.

(2) For the same subject the median nerve was stimulated electrically at the left wrist. From MEG data of left hand stimulus the dipole pattern of cSI was obtained and shown in Fig. 16.

Comparing Fig. 16 with Fig. 6 of the 53th component of BSS, we can conclude that the position of iSI in the right median nerve stimulus is the same as that of cSI in the left median nerve stimulus.

(3) It should be noted that time series data used for the identification method of feedback system theory were those of SQUIDs, $[\boldsymbol{x}(n)\boldsymbol{x}(n-1)\boldsymbol{x}(n-2)\cdots]$, or estimated time series data of current dipoles of SIs, $[\boldsymbol{y}(n)\boldsymbol{y}(n-1)\boldsymbol{y}(n-2)\cdots]$. Actual data of currents in the thalamus, $f_1(n)$ and $f_2(n)$, are not observable in measurement. Therefore we have no way to determine transfer functions $F_1(z^{-1})$ and $F_2(z^{-1})$ from Eq. (15) in our method, though $F_{12}(z^{-1})$ and $F_{21}(z^{-1})$ can be obtained from Eq. (14) as mentioned in Appendix B.

(4) Though the same trials for identification of dynamical activities between SIs were done in [15,27], we could not succeed to find the single dipole pattern of iSI by using kT type of BSS. It is important to use the T/k type of BSS for detection of iSI dipole pattern as mentioned in [2,22]. Furthermore, it should be noted that the time delay of about 30 ms was not detected without mapping to time series data of current dipoles from SQUIDs data.

(5) Since the arctan is a periodical function with period π and we cannot specify a positive or negative direction in fluctuations with zero mean, the sign of θ in $\boldsymbol{Q}_r(n) = Q_r(n)(\cos\theta\boldsymbol{i} + \sin\theta\boldsymbol{j})$ cannot be determined in identification of fluctuations. This sign ambiguity induces two possibilities in $y(n)$: one is a parallel case; $[y_1(n)y_2(n)]^T$ and the other is an antiparallel case; $[-y_1(n)y_2(n)]^T$. From this ambiguity we have another feedback model,

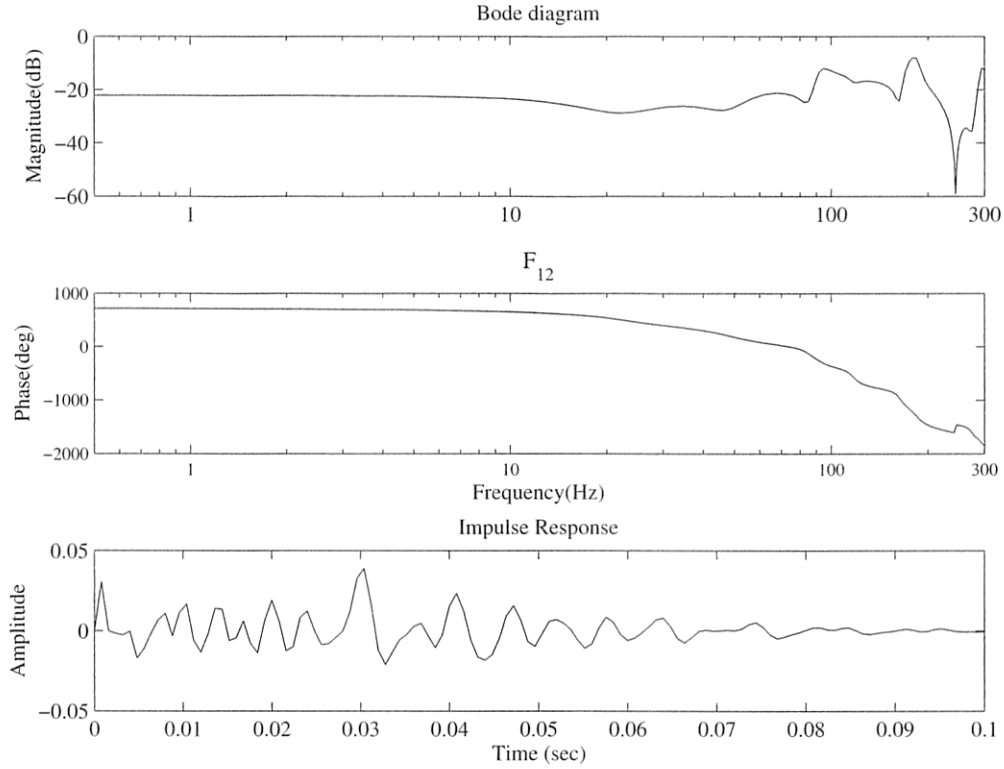

FIG. 15. Reproducibility of $\hat{F}_{12}$ from cSI to iSI and its impulse response.

$$y_1(n) = F_{12}^a(z^{-1})y_2(n) - F_1(z^{-1})f_1(n),$$

$$y_2(n) = F_{21}^a(z^{-1})y_1(n) + F_2(z^{-1})f_2(n), \tag{16}$$

where $F_{12}^a(z^{-1}) = -F_{12}(z^{-1})$ and $F_{12}^a(z^{-1}) = -F_{12}^a(z^{-1})$. Therefore there exists a sign ambiguity in the transfer function $F_{12}(z^{-1})$ or $F_{12}^a(z^{-1})$ in identification of fluctuations since the sign of amplitude of fluctuations of cSI and iSI cannot be determined from time series data. However, we have

$$\det\begin{pmatrix} 1 & -F_{12}^a(z^{-1}) \\ -F_{21}^a(z^{-1}) & 1 \end{pmatrix} = \det\begin{pmatrix} 1 & F_{12}(z^{-1}) \\ F_{21}(z^{-1}) & 1 \end{pmatrix}$$
$$= 1 - F_{12}(z^{-1})F_{21}(z^{-1})$$
$$= \det\begin{pmatrix} 1 & -F_{12}(z^{-1}) \\ -F_{21}(z^{-1}) & 1 \end{pmatrix},$$

in both cases of Eqs. (11) and (16). Hence it should be noted that the minimum phase properties of Eq. (A4) hold even in the sign ambiguity.

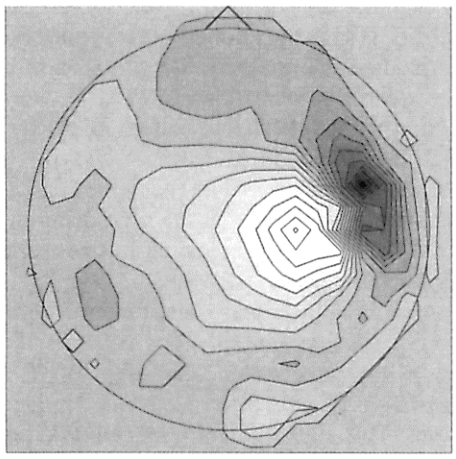

FIG. 16. (Color online) Dipole pattern of cSI in the case of left median nerve stimilus.

(6) We may expect that $s_{13}^{(7)}(n) \approx Q_{8618}(n)$ and $s_{53}^{(7)}(n) \approx Q_{7851}(n)$ since their dipole patterns of Figs. 4 and 5 are similar to those of the 53rd and 13th components in Fig. 6. Of course, current dipoles of SIs, $[Q_{7851}(n)Q_{8618}(n)]^T$, are different from the SEF components of BSS, $[s_{53}^{(7)}(n)s_{13}^{(7)}(n)]^T$, since $Q_{7851}(n)$ and $Q_{8618}(n)$ are real variables of current dipoles and $s_{13}^{(7)}(n)$ and $s_{53}^{(7)}(n)$ are abstract variables of BSS. However, it should be noted that we can find the same time delay in averaged waveforms of $s_{13}^{(7)}(n)$ (solid line) and $s_{53}^{(7)}(n)$ (broken line) in Fig. 17 as those in Fig. 12.

(7) The pathway of primary somatosensory cortices is still an open problem although we could find the time delay from cSI to iSI in the fluctuation analysis of MEG. In the case of the subject the pathway of SIs is transcallosal type. However, another subject as in [28] had direct afferent projection from thalamus.

In [12,28] this problem was studied by averaged waveforms on SQUID level as in Fig. 1. In [13] it was studied by averaged waveforms of current dipoles estimated from electroencephalography via the BSS method. In the present paper

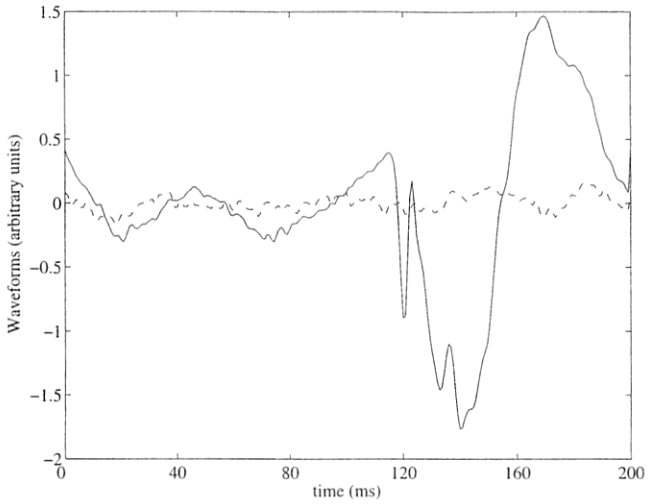

FIG. 17. Averaged waveforms of the 13th (solid line) and 53th (broken line) components of BSS.

we have studied it by impulse responses identified from fluctuations of current dipoles as mentioned above. It can be pointed out that the time delay of Fig. 12 in the current dipole level is not observed in SQUID waveforms of Fig. 1 and observed in BSS waveforms of Fig. 17.

(8) Simulation studies on estimation in the inverse formalism with combinatory optimization problem for location of current dipoles in Sec. II C were reported in [23]. The identification method with the feedback model of Eq. (11) in Sec. III could work on artificially prepared data that included known transfer functions in [25].

(9) Since there are multi-processing steps to obtain impulse responses in the present approach, we will examine whether obtained impulse responses are robust or not. To obtain impulse responses BSS is first applied to MEG data and then the elimination of the deterministic part is operated before the feedback model identification.

On the other hand, we may have an honest way to obtain impulse responses. In the honest way BSS is operated after the elimination of concatenation of 500 copies of averaged waveforms. From the Wold decomposition theorem, a stationary process is uniquely decomposed into deterministic and nondeterministic parts. Then SQUID data after elimination of deterministic part are fluctuations of nondeterministic part: SQUID fluctuations of the honest way were obtained from the same MEG data as mentioned in Sec. II by the elimination of concatenation of 500 copies of averaged waveforms. After elimination of the deterministic part, BSS with $k=7$ has been applied to them and the 13th and 53rd BSS components could be obtained for the contralateral and ipsilateral somatosensory primary cortexes from their dipole patterns. SQUID SEF fluctuations, $\boldsymbol{b}_e^h(n)$ have been obtained from the 13th and 53rd BSS components as in the same manner as Eq. (6). Next, the four current dipoles at positions 2366, 7876, 8001, and 8618 have been estimated by the same method mentioned in Sec. II B. The cSI and iSI dipoles were at 8618 and 7876. The location of iSI is a little different from that in the original way. Scalar time series data of four current dipoles have been obtained as in the similar manner as Eq. (9): $Q_e^h(n)=\boldsymbol{L}_e^{\dagger}\boldsymbol{b}_e^h(n)$. Finally, we have applied the feedback model identification mentioned in Sec. III to SEF fluctuations of cSI and iSI. The identified innovation model with minimum phase property could be calculated when the number of singular values of Hankel matrices was 23. Hence, the impulse response from cSI to iSI is shown in Fig. 18. The observed delay appears at about 30 ms in the impulse response. The consistency in the apparent delay for the single subject shows its robustness.

V. CONCLUSION

We have examined dynamical activities of cortices by magnetoencephalography study. In our methodology there are three procedures:

(1) The decorrelation method with T/k type time delayed is used for separation of evoked fields $\boldsymbol{b}_e(n)$ generated by somatosensory cortices.

(2) Inverse problem from SQUID SEF data $\boldsymbol{b}_e(n)$ to current dipole data $\boldsymbol{Q}_e(n)$ is solved by the multidipole estimation with combinatory optimization problem.

(3) Dynamical activities between primary somatosensory cortices can be examined from fluctuations of $y_1(n)$ and $y_2(n)$ after elimination of periodical waveforms by using the identification method based on feedback system theory.

In 5 Hz periodical median nerve stimulus somatosensory activities were examined. The iSI activity was found in Fig. 6 by using the T/k-type decorrelation method. Dynamical activities between primary somatosensory cortices were examined by using a feedback model with transfer functions. The time delay of about 30 ms has been detected in the impulse response from cSI to iSI by the blind identification method of Appendixes A and B.

ACKNOWLEDGMENTS

The author would like to thank Professor K. Shinosaki for providing MEG data, Professor Y. Yokota for valuable discussions on multidipole estimation, H. Kajita for help of MRI representation, and referees for their useful comments. This work was supported by Grant-in-Aid for Scientific Research (Grant No. 19500237) of Japan Society for the Promotion of Science.

APPENDIX A: INNOVATION MODEL IN STATISTICAL INVERSE PROBLEM

In [7,25,29] our identification formalism has been summarized as five steps to obtain numerically an innovation model of Eq. (12):

Step 1: calculate correlation function matrices $R_{yy}(k)$ from N time series data, $\boldsymbol{y}(n)=[y_1(n)y_2(n)]^T$, $(n=1,2,\ldots,N)$:

$$R_{yy}(k)=\frac{1}{N}\sum_{j=1}^{N-k}(\boldsymbol{y}(j+k)\boldsymbol{y}(j)^T),$$

where the mean is assumed to be zero, i.e., $E\{\boldsymbol{y}(n)\}=\frac{1}{N}\sum_{j=1}^{N}\boldsymbol{y}(j)=0$.

Step 2: define a Hankel matrix $H_{yy}(k)$, and its associate matrices, $H_A(k)$, $H_B(k)$, and $H_C(k)$ as

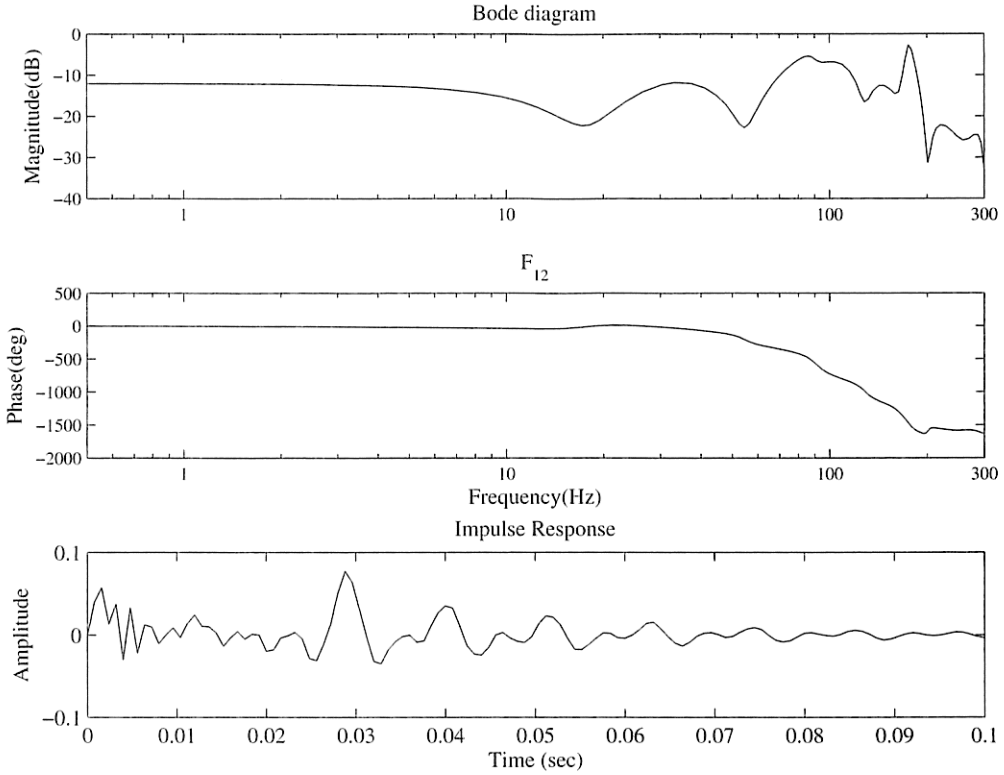

FIG. 18. Reproducibility of $\hat{F}_{12}$ from cSI to iSI and its impulse response in the honest way.

$$H_{yy}(k) := \begin{pmatrix} R_{yy}(0) & R_{yy}(1) & \cdots & R_{yy}(k) \\ R_{yy}(1) & R_{yy}(2) & \cdots & R_{yy}(k+1) \\ \vdots & \vdots & & \vdots \\ R_{yy}(k) & R_{yy}(k+1) & \cdots & R_{yy}(2k) \end{pmatrix},$$

$$H_A(k) := \begin{pmatrix} R_{yy}(1) & R_{yy}(2) & \ldots & R_{yy}(k+1) \\ R_{yy}(2) & R_{yy}(3) & \ldots & R_{yy}(k+2) \\ \vdots & \vdots & & \vdots \\ R_{yy}(k+1) & R_{yy}(k+2) & \ldots & R_{yy}(2k+1) \end{pmatrix},$$

$$H_B(k) := \begin{pmatrix} R_{yy}(0) \\ R_{yy}(1) \\ \vdots \\ R_{yy}(k) \end{pmatrix},$$

$$H_C(k) := [R_{yy}(0) R_{yy}(1) \cdots R_{yy}(k)].$$

Step 3: calculate three matrices A, B_q, and C from the associated matrices, $H_A(k)$, $H_B(k)$, and $H_C(k)$ by using the singular value decomposition of the Hankel matrix H_{yy}. That is, we have

$$A_H = \Sigma_k^{-1/2} U_k^T H_A(k) V_k \Sigma_k^{-1/2},$$

$$B_q = \Sigma_k^{-1/2} U_k^T H_B(k),$$

$$C = H_C(k) V_k \Sigma_k^{-1/2}, \tag{A1}$$

where $H_{yy}(k) = U_k \Sigma_k V_k^T$, Σ_k is a diagonal matrix of which the diagonal elements consist of d positive singular values and $2(k+1)-d$ zeros, and U_k and V_k are orthogonal matrices.

Step 4: a stable solution of matrix Riccati equation can be calculated by iteration procedures:

$$E_{n+1} = A_H E_n A_H^T + A_H K_n (B_q - E_n C^T)^T A_H^T, \tag{A2}$$

where $K_n = (B_q - E_n C^T)(R_{yy}(0) - C E_n C^T)^\dagger$. We obtain B from B_q and a stable solution E_∞ of Eq. (A2),

$$B := K_\infty = (B_q - E_\infty C^T)(R_{yy}(0) - C E_\infty C^T)^\dagger.$$

Discussions to find a stable solution of the matrix Riccati equation were reported theoretically in [6,7,29] and numerically in [25,30,31].

Step 5: finally we have a d-dimensional data-oriented innovation model,

$$\boldsymbol{x}(n|n) = A_H \boldsymbol{x}(n-1|n-1) + B\boldsymbol{\gamma}(n)$$

$$\boldsymbol{y}(n) = C\boldsymbol{x}(n|n), \tag{A3}$$

where $\boldsymbol{\gamma}(n) := \boldsymbol{y}(n) - \boldsymbol{y}(n|n-1)$. Here $\boldsymbol{y}(n|m)$ is the conditional mean value of $\boldsymbol{y}(n)$ under the condition that $[\boldsymbol{y}(m)\boldsymbol{y}(m-1)\boldsymbol{y}(m-2)\cdots]$ are given: $\boldsymbol{y}(n|n-1) := E\{\boldsymbol{y}(n)|\boldsymbol{y}(n-1)\boldsymbol{y}(n-2)\boldsymbol{y}(n-3)\cdots\}$. Coefficient matrices of the data-oriented innovation model have the minimum phase property of pole stability and zero invertibility,

$$\text{eig}|A_H| < 1 \text{ and } \text{eig}|A_H(I - BC)| < 1. \tag{A4}$$

APPENDIX B: EVALUATION OF TRANSFER FUNCTIONS IN FEEDBACK MODEL

From the data-oriented innovation model [Eq. (A3)] we have closed loop transfer functions $G_{ij}(z^{-1})$:

$$\begin{pmatrix} G_{11}(z^{-1}) & G_{12}(z^{-1}) \\ G_{21}(z^{-1}) & G_{22}(z^{-1}) \end{pmatrix} := C(I - A_H z^{-1})^{-1} B. \quad \text{(B1)}$$

Transfer functions of Eq. (11), $F_{ij}(z^{-1}) := C_{ij}(I - A_{ij}z^{-1})^{-1}B_{ij}z^{-1}$, can be identified from Eq. (B1) under two sufficient conditions of minimum phase and independence of random variables [6,7], which are similar to results mentioned in [32,33]. When the feedback structure of Eq. (11) is conserved under the sufficient condition, the data-oriented innovation model can be evaluated as

$$y_1(n) = \hat{F}_{12}(z^{-1})y_2(n) + \hat{F}_1(z^{-1})\gamma_1(n)$$

$$y_2(n) = \hat{F}_{21}(z^{-1})y_1(n) + \hat{F}_2(z^{-1})\gamma_2(n), \quad \text{(B2)}$$

where transfer functions of $\hat{F}_{12}(z^{-1})$ and $\hat{F}_{21}(z^{-1})$ are determined by a transformation from closed loop transfer functions [6,7,19,25]:

$$\hat{F}_{12}(z^{-1}) = G_{12}(z^{-1})G_{22}(z^{-1})^{-1},$$

$$\hat{F}_{21}(z^{-1}) = G_{21}(z^{-1})G_{11}(z^{-1})^{-1}. \quad \text{(B3)}$$

[1] M. Hämäläinen, R. Hari, R. J. Ilmoniemi, J. Knuutila, and O. V. Lounasmaa, Rev. Mod. Phys. **65**, 413 (1993).
[2] K. Kishida, Phys. Rev. E **79**, 011922 (2009).
[3] G. Gomez-Herrero, M. Atienza, K. Egiazarian, and J. L. Cantero, Neuroimage **43**, 497 (2008).
[4] C. Porcaro, F. Zappasodi, P. M. Rossini, and F. Tecchio, Electroencephalogr. Clin. Neurophysiol. **120**, 436 (2009).
[5] K. Kishida, Proceedings of the 11th IFAC Symposium on System Identification (1997), p. 1437.
[6] K. Kishida and N. Suda, J. Nucl. Sci. Technol. **31**, 526 (1994).
[7] K. Kishida, in *Advances in Nuclear Science and Technology*, edited by J. Lewins and M. Becker (Plenum, New York, 1996), Vol. 23, pp. 1–68.
[8] H. Wikström, J. Huttunen, A. Korvenoja, J. Virtanen, O. Salonen, H. Aronen, and R. J. Ilmonniemi, Electroencephalogr. Clin. Neurophysiol. **100**, 479 (1996).
[9] R. Kakigi, M. Hoshiyama, M. Shimoto, D. Naka, H. Yamasaki, S. Watanabe, J. Xiang, K. Maeda, K. Lam, K. Itomi, and A. Nakamura, Prog. Neurobiol. **61**, 495 (2000).
[10] M. Boakye, S. C. Huckins, N. M. Szeverenyi, B. I. Taskey, and C. J. Hodge, Jr., J. Neurosurg. **93**, 774 (2000).
[11] T. Nihashi, S. Naganawa, C. Sato, H. Kawai, T. Nakamura, H. Fukatsu, T. Ishigaki, and I. Aoki, Clin. Neurophysiol. **116**, 842 (2005).
[12] A. Kanno, M. Nakasato, K. Hatanaka, and T. Yoshimoto, Neuroimage **18**, 169 (2003).
[13] M. T. Sutherland and A. C. Tang, Neuroimage **33**, 1042 (2006).
[14] J. Sarvas, Phys. Med. Biol. **32**, 11 (1987).
[15] K. Kishida, K. Kato, K. Shinosaki, and S. Ukai, Proceedings of the Fourth International Symposium on Independent Component Analysis and Blind Signal Separation (ICA2003) (2003), p. 185.
[16] L. Molgedey and H. G. Schuster, Phys. Rev. Lett. **72**, 3634 (1994).
[17] A. Ziehe, K. R. Müller, G. Nolte, B. M. Mackert, and G. Curio, IEEE Trans. Biomed. Eng. **47**, 75 (2000).
[18] N. Murata, S. Ikeda, and A. Ziehe, Neurocomputing **41**, 1 (2001).
[19] K. Kishida, H. Fukai, T. Hara, and K. Shinosaki, IEICE Trans. Fundamentals **86-A**, 611 (2003).
[20] A. C. Tang, M. T. Sutherland, and C. J. McKinney, Neuroimage **25**, 539 (2005).
[21] N. Hironaga and A. A. Ioannides, Neuroimage **34**, 1519 (2007).
[22] K. Kishida, in *Biomagnetism: Interdisciplinary Research and Exploration*, edited by R. Kakigi, K. Yokosawa, and S. Kuriki (Hokkaido University Press, Sapporo, 2008), pp. 124–126.
[23] Y. Yokota and K. Kishida, IEICE Trans. Fundamentals **J89-A**, 1108 (2006) (in Japanese).
[24] J. Mosher, P. S. Lewis, and R. M. Leahy, IEEE Trans. Biomed. Eng. **39**, 541 (1992).
[25] K. Kishida, J. Nucl. Sci. Technol. **34**, 1115 (1997).
[26] Y. Hlushchuk and R. Hari, J. Neurosci. **26**, 5819 (2006).
[27] K. Kishida, Proceedings of IEEE International Symposium on Circuits and Systems (ISCAS), 2005, p. 5694.
[28] A. Kanno, N. Nakasato, Y. Nagamine, and T. Tominaga, J. Clin. Neurosci. **11**, 868 (2004).
[29] K. Kishida, J. Math. Phys. **32**, 92 (1991).
[30] K. Kishida, Proceedings of ISM Symposium on Statistical Researches in Complex Systems (2001), p. 65.
[31] K. Kishida and S. Masuda, Proceedings of the 33rd ISCIE International Symposium on Stochastic Systems Theory and Its Applications (2002), p. 222.
[32] G. C. Goodwin and R. L. Payne, *Dynamic System Identification: Experiment Design and Data Analysis*, Mathematics in Science and Engineering, Vol. 136 (Academic, New York, 1977).
[33] T. S. Ng, G. C. Goodwin, and B. D. O. Anderson, Automatica **13**, 477 (1977).